



ELSEVIER

Nuclear Instruments and Methods in Physics Research A 447 (2000) 536–543

**NUCLEAR
INSTRUMENTS
& METHODS
IN PHYSICS
RESEARCH**
Section A

www.elsevier.nl/locate/nima

New design features of gas ionization detectors used for elastic recoil detection

H. Timmers^{a,b,c}, R.G. Elliman^b, T.R. Ophel^{c,*}

^a*Department of Physics, University of Newcastle, Callaghan, NSW 2308, Australia*

^b*Department of Electronic Materials Engineering, Research School of Physical Sciences and Engineering,
Australian National University, Canberra, ACT 0200, Australia*

^c*Department of Nuclear Physics, Research School of Physical Sciences and Engineering, Australian National University,
Canberra, ACT 0200, Australia*

Received 18 August 1999; received in revised form 8 November 1999; accepted 20 November 1999

Abstract

Several alternative design features of large acceptance, gas ionization detectors have proven to be successful for application to elastic recoil detection analysis (ERDA). In particular, effects due to the distortion of the entrance field by a large area window have been eliminated in a simple fashion, to allow measurement of the initial rate of energy loss and to provide an energy- and species-independent cathode signal. No less importantly, use of a divided electrode in the anode plane has enabled a more straightforward means of determining the scattering angle that is required for kinematic corrections. An intermediate grid was found to provide a direct and true total energy signal, with only slightly diminished resolution compared with that of the summed total anode equivalent. © 2000 Elsevier Science B.V. All rights reserved.

PACS: 29.40.Cs; 29.40.Gx; 81.70.Jb; 81.70.Yb

Keywords: Ion beam analysis; Elastic recoil detection

1. Introduction

Large solid-angle ionization detectors have been used effectively for elastic recoil analysis of thin films with heavy-ion beams [1–3]. Typically though, kinematic correction of measured data, an essential feature needed because of the large angular acceptance of the detectors, is neither straightforward nor optimal. This unsatisfactory situation arises from the commonly used technique whereby

signals from a divided cathode electrode provide the means to determine both orthogonal coordinates of ion trajectories. Separation of the inter-related coordinates is complicated by ion species and energy-dependent non-linearities that are evident in the total cathode signal. Moreover the sensitivity, and therefore the achievable transverse spatial resolution, of a divided cathode decreases quadratically as the distance of the ion path from the cathode increases.

Recently, the performance of a multi-anode ionization detector was investigated in detail [3]. It was found that distortion of the entrance field by a large area window was responsible for a

*Corresponding author. Tel.: +61-6-2492086; fax: +61-6-2490748.

E-mail address: tro103@nuc.anu.edu.au (T.R. Ophel).

species- and energy-dependent deficit in the cathode signal, thus accounting for the difficulties encountered previously. Entrance field effects also influence the longitudinal collection of electrons by the anode. Measurements of the initial energy loss of ions within the detector showed a substantial variation which was related to the distance of the ion path from the cathode, even though the total anode signal was unaffected.

A number of alternative design features were proposed in Ref. [3]. In principle, they are capable of providing species- and energy-independent spatial measurements, as well as overcoming the problems associated with the measurement of the initial rate of energy loss. In the present work, some of those options have been implemented and evaluated. A summary of preliminary results was reported recently [4].

2. Experimental details

The electrode structure of the detector described in Ref. [3] has been substantially modified (Fig. 1). Rather than attempting the complex task of voltage-grading the thin window ($\sim 70 \mu\text{g cm}^{-2}$), the entrance geometry was changed to provide an acceptable field configuration. The window was relocated vertically off-axis, 10 mm closer to the Frisch grid, and withdrawn from within the electrodes (previously 3.6 mm inside) to be 2.6 mm in front of the leading edge of the ΔE_1 electrode. Further, an undivided cathode was truncated by eliminating the front 30 mm, corresponding to the width of the ΔE_1 electrode. Two-dimensional field calculations were made for the modified entrance geometry, assuming that the entire window assembly could be treated as an equipotential at the applied window voltage because of the supporting grid. Earlier results were consistent with this assumption, the validity of which was evidently assisted by the voltage-graded guard wires flanking the length of the gap between the cathode and the Frisch grid. The combination of having the window withdrawn and off-axis, along with the truncated cathode, yields equipotentials that are near-parallel to the grid at the junction between the ΔE_1 and ΔE_2 electrodes, allowing an estimate that the vari-

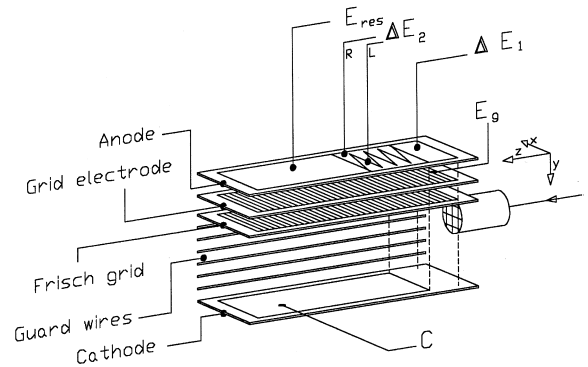


Fig. 1. The modified detector configuration showing the original ΔE_2 section of the anode divided into sawtooth segments and the entire cathode truncated by an amount equivalent to the width of the ΔE_1 electrode. A separation of 70 mm between the cathode and the Frisch grid was retained.

ation of the ΔE_1 signal with distance from the cathode should be significantly less than 5% for the full detector aperture.

The basic anode structure of three sections remained the same, with ΔE_1 , ΔE_2 and E_{res} electrodes that were 30, 60 and 120 mm long, respectively. However, the ΔE_2 electrode was converted to a sawtooth configuration to derive directly the horizontal, in-plane coordinate (x) of each event, independently of the out-of-plane, vertical coordinate (y). The latter coordinate, to be obtained from the ratio of the cathode signal to the sum of those from the ΔE_2 and E_{res} electrodes, could be anticipated to be free of ion species and energy dependencies on the basis of the results previously reported [3].

In parallel with the detector re-design to simplify position derivation, a second grid electrode was installed as an electrode between the original Frisch grid and the anode plane. The two grids were 10 mm apart, with the anode plane a further 10 mm above the second grid. It was hoped that the additional grid would provide a useful direct, total energy signal of adequate resolution, even though the triangular pulse shape that will result is likely to lead to some dependence of the response on the orientation of the ion trajectory. Previous use of double grids would seem to have been rather limited. A number of focal plane detectors within magnetic spectrometers employed a second grid,

between the cathode and a Frisch grid, which was capacitively coupled to the cathode to derive a total energy signal [5,6]. As pointed out in Ref. [3], such a signal in fact suffers a deficit due to entrance field distortion too. A similarly located grid was used by Ogawa et al. [7] to “collimate electronically” alpha-particles in order to minimize source thickness effects. Sann et al. [8] demonstrated that a grid between the anode and a Frisch grid could provide spatial information. No attempt was made in that work to obtain energy-related information though, while delays between the individual grid wires were used to extract a position measurement. Nonetheless, it was clear that allowing the voltage of the additional grid to vary did not have a significant effect on the quality of the anode signals. Some results obtained with the grid electrode have been presented elsewhere [9].

Measurements were made at a scattering angle of 45° with a variety of targets, using beams of ^{16}O at 30 MeV and of ^{197}Au at 214 and 241 MeV. A rectilinear mask, comprised of nine holes, 1 mm in diameter and 5 mm apart [3], was used to investigate the spatial properties of the various signals in detail.

3. Results and discussion

3.1. The window geometry

Measurements of the anode signals were made with the mask using 30 MeV ^{16}O ions scattered from a thin ^{197}Au target. The combined results for all nine holes of the mask yielded resolutions of 6% for ΔE_1 , 4% for ΔE_2 , 6.6% for E_{res} and 1.2% for the total energy, where ΔE_2 was the sum of the two sawtooth segments, and the total energy the sum of all four anode signals after gain adjustment. Ready identification of the individual holes was obtained from the cathode and the divided ΔE_2 electrode signals. A detailed discussion of these signals follows in Sections 3.2 and 3.3.

The total energy resolution improved to 0.9% for the central column of apertures (Fig. 2), consistent with the elimination of the kinematic variation of ~ 120 keV across the 10 mm spanned by the mask. Thus the overall noise is ~ 260 keV, indicating that

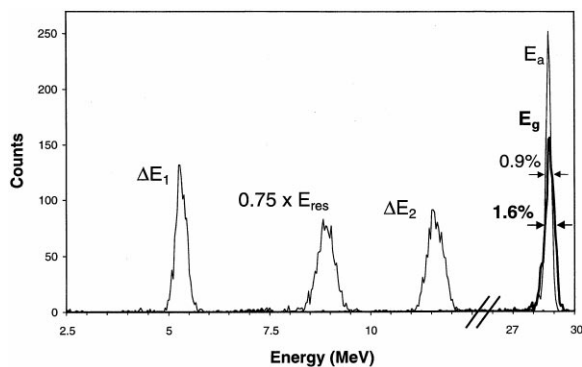


Fig. 2. Spectra of the various signals obtained with the detector for 30 MeV ^{16}O ions scattered from ^{197}Au . The measurement was made with the rectilinear mask in front of the detector. The data shown are from only the central column of holes that span 10 mm. The summed anode signal is designated E_a . For completeness, the total energy signal from the grid electrode, E_g , is also shown. The latter is discussed in Section 3.4.

the ΔE_1 resolution is mainly noise-limited, whereas the resolutions of both ΔE_2 and E_{res} reflect straggling effects.

Significantly, the ΔE_1 resolution for either the central column or the full aperture was little different from that obtained for only the central hole of the mask. In fact, the vertical variation of the ΔE_1 centroid over the central 10 mm spanned by the mask was typically less than 2.5%. Clearly, the effects of field distortion due to the entrance window on the collection of electrons by the anode have been eliminated.

Recoil spectra obtained with the full detector aperture of 20 mm diameter for a thin film of the high-temperature superconductor $\text{YBa}_2\text{Cu}_3\text{O}_{7-x}$ (deposited on a MgO substrate) are shown in Fig. 3. The resolution for the Cu group within the projected ΔE_1 spectrum is $\sim 6.3\%$, confirming the integrity of the signal for actual ERDA measurements.

The benefits of an additional, initial energy loss signal have already been demonstrated [2]. Comparison of Fig. 3 and measurements of ΔE_2 with the same sample that are given in the following section (Fig. 6) further illustrates the value of such a measurement. The ΔE_1 signal gives clean separation of a wide range of ion species and energies, otherwise only possible by measurements at several different detector gas pressures.

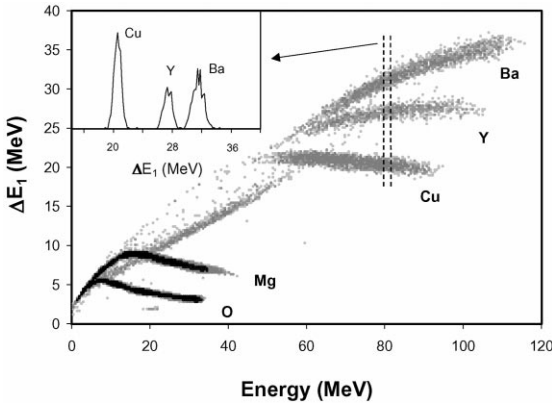


Fig. 3. A contour projection of ΔE_1 versus total energy for a thin superconducting film deposited on a substrate of MgO measured with the full detector aperture. The energy loss distribution of Cu, Y and Ba ions for the indicated energy window is shown in the inset. A ^{197}Au beam was used at 241 MeV.

Since the field variations have been reduced substantially, timing between the cathode signal and one of the anode signals would become feasible as an alternative technique to determine the distance of the ion trajectory from the cathode. The distorted entrance field of earlier geometries would cause considerable time jitter on the cathode signal. It will be shown in Section 3.4 that an equivalent configuration, with the window located in the lower half of the detector, should be preferable for the application of this technique.

3.2. The sawtooth ΔE_2 anode electrode

One essential difference between the alternative sawtooth configurations is immediately apparent in Fig. 4. Whereas the signals from the segments of a cathode sawtooth were different for all nine mask holes, those of the anode sawtooth are sensitive only to the displacement of the ions in the x direction. Hence the three vertical columns of the mask are readily separated. The energy resolution for each segment was typically $\sim 7\%$, while that of the summed ΔE_2 signal was $\sim 5\%$. For 30 MeV ^{16}O ions scattered from a thin ^{197}Au target, the effective x -resolution was 0.8 mm, based on the separation of the mask holes. The actual resolution is somewhat larger of course because the outer trajectories defined by the mask are diverging from

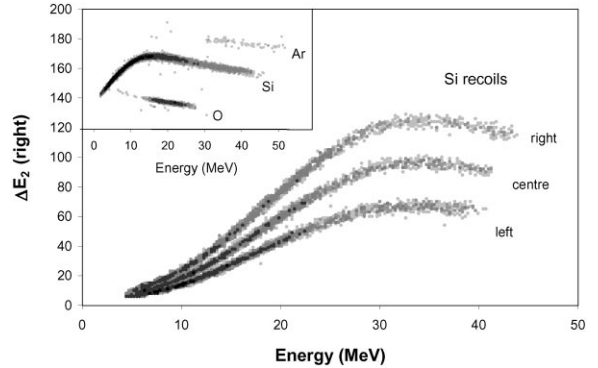


Fig. 4. The ΔE_2 (right) versus total energy projection obtained for ^{28}Si ions with energies ranging between about 5 and 45 MeV from a sample of SiO_2 bombarded with 214 MeV ^{197}Au ions. The measurement was made with the mask in front of the detector. The differences of the total energy endpoints stem from the kinematic variation across the central 10 mm of the detector. The inset (ΔE_1 versus energy) indicates the sample composition.

the target. The improved resolution from an anode sawtooth stems mainly from the y -independent ratio of the left and right ΔE_2 signals of ~ 1.8 for a 5 mm displacement. This ratio corresponds closely to that expected from the geometrical difference between the path lengths. In contrast, a cathode sawtooth of identical pitch yielded a ratio of only ~ 1.2 for similar in-plane trajectories, and even smaller values for ions above the plane [3]. Moreover, location of the anode sawtooth in the front region of the detector minimizes multiple scattering effects which become significant at the end of ion ranges.

Although in principle, use of a sawtooth for only part of the anode reduces the energy range of ions for which spatial information can be extracted, it is clear from Fig. 4 that any reduction is relatively small and of no consequence for surface analysis. The data given were obtained with a 214 MeV ^{197}Au beam, for which the maximum ^{28}Si recoil energy is ~ 46.5 MeV. For typical operating conditions, ^{28}Si ions with energies of 10 MeV and below still provide a useful ΔE_2 signal, though the position resolution is diminished.

For any sawtooth configuration, the detailed spatial response is affected by the manner in which the energy loss of the ions varies as a function of distance along the trajectory in the gas. Unless the

change of the rate of energy loss is near-linear and the ion passes beyond the ΔE_2 electrode, the signals from the two segments will differ slightly even for a central trajectory. The magnitude of such a difference will depend on the pitch of the sawtooth, and the degree of range straggling for particular ions if they are stopped under ΔE_2 . In the case of a cathode sawtooth, neither effect can be eliminated. With an anode sawtooth, the gas pressure could be selected either to minimize or eliminate both, although it will be seen that any uncertainties that result in the extracted position information are small (~ 1 mm) and generally occur for ions with energies below the region of interest.

The response of the anode sawtooth was examined using the mask for recoil ions from a thin (~ 10 nm) silicon dioxide layer on a silicon substrate, onto which a second, thin (also ~ 10 nm) layer of titanium and germanium had been co-deposited. For central trajectories, the amplitudes of the signals from the two segments (designated left and right) were essentially identical for the oxygen ions (~ 30 MeV) and the highest energy silicon ions (~ 46 MeV), but the ratio (left/right) fell below unity for the lower energy silicon ions, and for the titanium and germanium ions (~ 63 and 78 MeV, respectively, although their ΔE_2 values are little different) (Fig. 5). The maximum departure of the silicon ions from linearity occurs for energies below 30 MeV. This behaviour, also evident for the flanking off-axis trajectories, is attributed to the fact that silicon ions below 30 MeV are almost stopped beneath the ΔE_2 electrode. Consequently, the variation of their energy loss under ΔE_2 is extreme. On the other hand, the variation for 30 MeV oxygen ions is relatively small and linear, while the rate of energy loss for the highest energy silicon ions (see Fig. 6) is almost constant (hence the grouping of events at the high energy limits of the silicon ions in Fig. 5). The initial section of the sawtooth electrode is associated with the left segment, so that any non-linearity of the energy loss under ΔE_2 would reduce the left/right ratio, consistent with observation. Clearly the effects, which correspond to a discrepancy of less than 1 mm in the measured displacement of the ion trajectory, are apparent for those ions only for energies which are not of interest in ERDA applications.

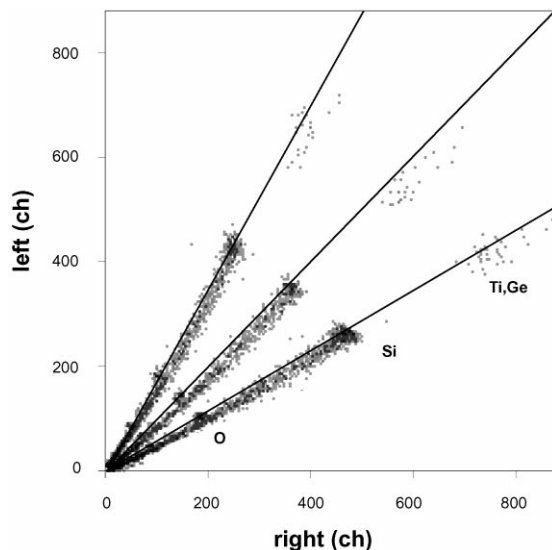


Fig. 5. A comparison of the left and right ΔE_2 signals for the indicated ion species using the mask (see text).

Another response anomaly, due also to the behaviour of dE/dx , becomes manifest for heavier ions at energies for which the energy loss under ΔE_2 increases rapidly with energy. Then the kinematic energy variation of the ions results in an asymmetry of the ΔE_2 signals about the central axis. An indication of such an asymmetry is suggested by the behaviour of the Ti and Ge ions in Fig. 5. However, the $\text{YBa}_2\text{Cu}_3\text{O}_{7-x}$ sample used above proved more useful to investigate the effect. Recoiling copper, yttrium and barium ions from from this sample are indeed associated with ΔE_2 values that change rapidly with energy (Fig. 6). A measurement with the full detector aperture indicates a rotation of events away from the 45° axis (Fig. 7), with the larger signals being on the right segment, which corresponds to the smaller scattering angles and therefore the higher incident energies. Correction is straightforward enough, though without it the error in the measured displacement is again only ~ 1 mm.

3.3. The truncated cathode

The response of the truncated cathode was found to be almost completely independent of the energy

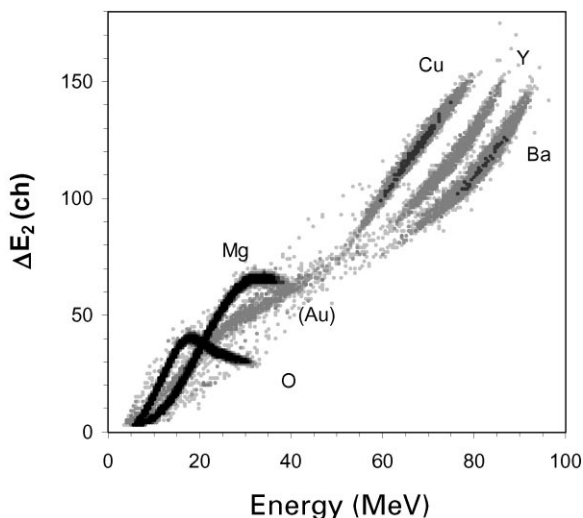


Fig. 6. The ΔE_2 versus energy projection for the same sample as in Fig. 3. However, in this case a beam energy of 214 MeV was used.

lost in the region before it. In particular, few of the ions stopping under the ΔE_1 electrode gave rise to a detectable, albeit small, signal. Thus for any ion trajectory parallel to the cathode, the truncated cathode configuration should be species-independent and exhibit a linear dependence on both the energy lost under the ΔE_2 and E_{res} electrodes, and the distance of the trajectory from the cathode. In fact, a near-quadratic dependence of the cathode signal on the distance between the ion trajectory and the cathode is observed [3]. Evidently, it arises because the amplifier time constants normally used are comparable to the range of variation of the rise times of the cathode signals. Thus, the integrated voltage output is influenced strongly by the duration of the change of cathode signal as well as by the magnitude of it. Both the magnitude and duration are linearly height-dependent. For diverging trajectories that obtain in actual use, the situation becomes more complex. The actual voltage variation and the rise time of the cathode signal will be affected by the variation of dE/dx along the ion path and by the ion range, leading to some species and energy dependence of the ratio cathode/ $(\Delta E_2 + E_{res})$.

A typical measurement with the mask (Fig. 8) illustrates the response of the cathode to oxygen

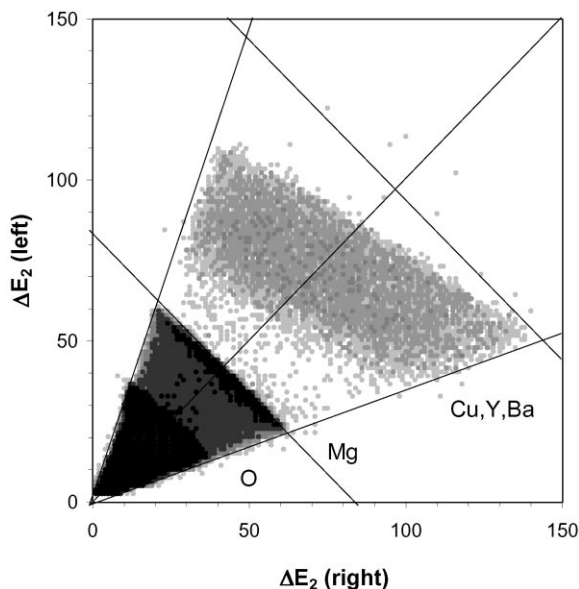


Fig. 7. Signals from the divided ΔE_2 anode obtained during the measurement of the data given in Fig. 6.

and silicon ions which span a considerable energy range. Satisfactory linearity is obtained for each of the three mask rows. Differences stemming from range and energy loss effects are small, being directly apparent only for the upper trajectories, even though the range of the highest energy ^{16}O ions is about 30% longer than that for silicon ions yielding the same $(\Delta E_2 + E_{res})$ signal. It is to be noted that the linearity observed with the truncated cathode confirms the notion of the cathode deficit proposed in Ref. [3]. Despite the energy linearity, it is evident in Fig. 8 that the cathode amplitudes for the upper and lower rows of the mask are not uniformly spaced about the value for the central ray, reflecting the previously observed non-linearity.

The height dependence of the cathode signal is more readily demonstrated at full aperture using 30 MeV ^{16}O ions elastically scattered from a thin ^{197}Au target (Fig. 9). Clearly, even for mono-energetic ions, a relatively large dynamic range of cathode signal prevails for the present detector configuration, being about twice that obtained with the window centrally located. Application of a square-root function to the asymmetric measured distribution results in a near-symmetric distribution,

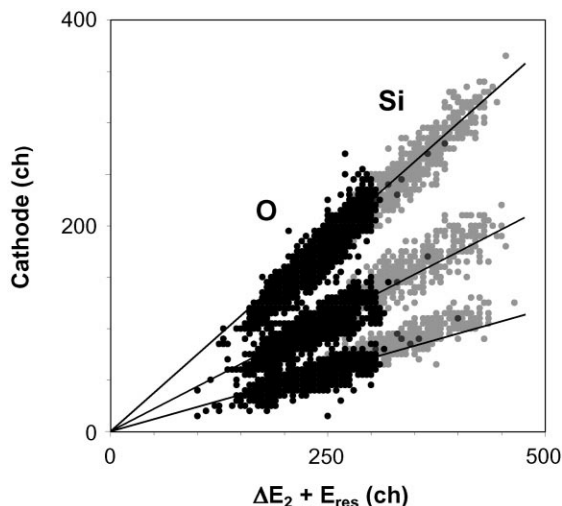


Fig. 8. A comparison of the cathode responses for ¹⁶O (black) and ²⁸Si (grey) ions using the mask. The measurement was obtained simultaneously with the data of Fig. 4.

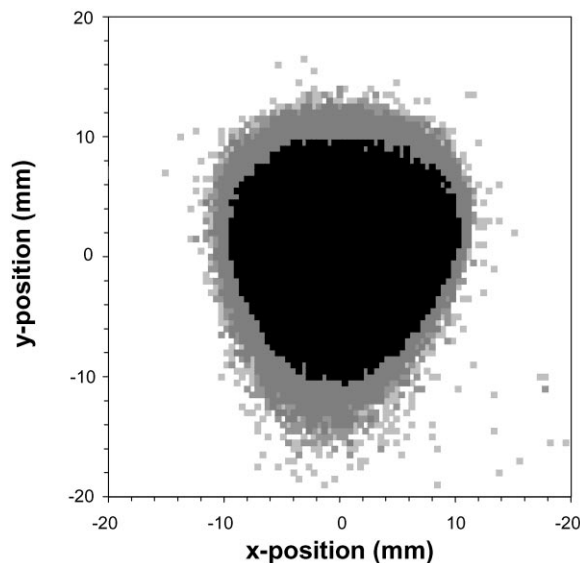


Fig. 10. A typical x-y projection for all ions, spanning elements between carbon and tin, entering the detector.

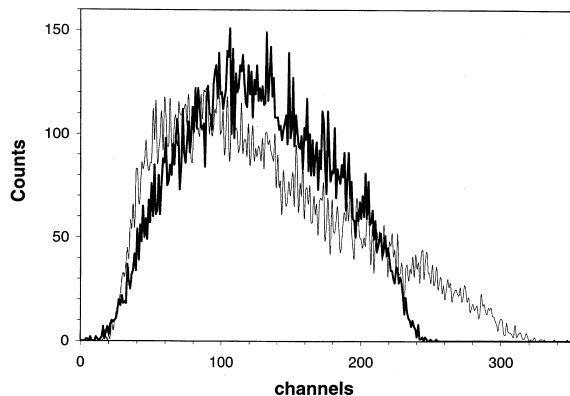


Fig. 9. The measured (thin) and corrected (thick) cathode pulse height distributions for mono-energetic 30 MeV ¹⁶O ions scattered from gold.

centred about a uniformly spaced mask pattern that eventuates after similar correction. Because of the combined effects of the resolution broadening that occurs over the wide range of cathode amplitudes, and of the use of a simple function to correct for the measured non-linearity, projections of y versus x are slightly distorted (Fig. 10).

As foreshadowed in Section 3.1, an alternative and near-equivalent entrance geometry, with the window 10 mm below the central axis, would retain

the y -independence of ΔE_1 , but also reduce the dynamic range of the cathode signal and therefore the distortion. The range of ~ 9 observed here would decrease to ~ 2.6 for this latter configuration, which could, however, not be implemented readily within the existing detector. The distortion is unimportant in the present application since determination of the y -coordinate is no longer a necessary prerequisite for kinematic correction, the in-plane scattering angle being established directly from the ΔE_2 sawtooth. Nonetheless, the x - y projection remains useful to allow some rejection of events that arise from large-angle scattering of ions by the stopping gas.

3.4. The second grid

With 375 and 750 V applied to the second grid and the anode, respectively, the pulse height of the signal obtained from the grid was about half that when the grid was operated at a high enough voltage to collect all of the electrons. Optimum resolution was achieved with short integration times because of the triangular pulse shape that obtains. Either 0.25 or 0.5 μ s was used, depending on the amplifier type. The variation of the pulse

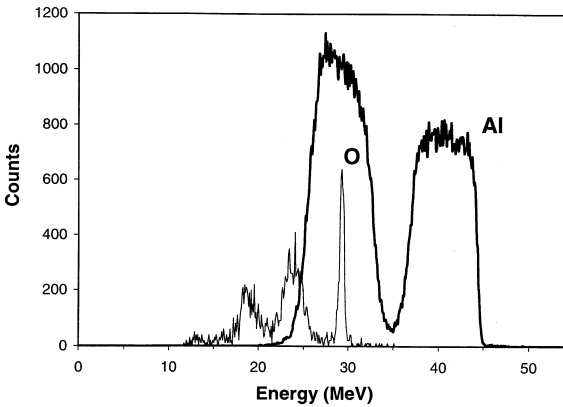


Fig. 11. Typical total energy spectra measured with the grid electrode (see text).

height over the central 10 mm diameter was found to be less than 0.5%, indicating that any dependence of the grid response to the orientation of the ion trajectory is minor. For measurements made with 30 MeV ^{16}O scattered from a thin ^{197}Au target, a resolution of 1.6% was obtained for the grid signal, when that from the summed total anode signal was 0.9% (Fig. 2). With actual samples, for which the resolution is largely determined by straggling and multiple scattering of both the incident beam and the exiting recoil ions, there was essentially no difference between the two total energy measurements [9]. Kinematically corrected energy distributions of recoil oxygen and aluminium ions measured with the grid electrode for a sample comprised of a 60 nm hydrocarbon layer sandwiched between aluminium layers 360 nm thick are shown in Fig. 11. Clearly, excellent surface resolution is achieved for both ion species.

The amplitude of the grid signal was found to be a function of the detector gas pressure if the electrode voltages were held constant. Such variation was eliminated by scaling the voltages with pressure.

As would be expected, the grid and the summed total anode signal are precisely correlated in a lin-

ear fashion, provided the gain matching of the four anode signals has been established correctly. In fact, departures from linearity serve as a further means to establish the matching.

4. Conclusion

A detector with significantly improved capabilities for ERDA measurements has been demonstrated. Kinematic correction is simple, being essentially ion species and energy independent. A wide range of elements can be identified cleanly at a single detector gas pressure, thus minimizing the duration of bombardment of samples. The introduction of an intermediate grid electrode to measure the total ion energy eliminates the need to sum the various anode signals in most applications. No less importantly, the techniques presented here to overcome the effects of entrance field distortion, and to obtain the scattering angle, can be implemented readily in detectors of substantially larger solid angle than are currently used.

References

- [1] W. Assmann, P. Hartung, H. Huber, P. Staat, H. Steffens, Ch. Steinhausen, Nucl. Instr. and Meth. B 85 (1994) 726.
- [2] J.S. Forster, P.J. Currie, J.A. Davies, R. Siegele, S.G. Wallace, D. Zelinsky, Nucl. Instr. and Meth. B 113 (1996) 308.
- [3] T.R. Ophel, H. Timmers, R.G. Elliman, Nucl. Instr. and Meth. A 423 (1999) 381.
- [4] H. Timmers, R.G. Elliman, T.R. Ophel, Nucl. Instr. and Meth. B (2000) in press.
- [5] H.W. Fulbright, J.R. Erskine, Nucl. Instr. and Meth. 162 (1979) 355.
- [6] T.R. Ophel, A. Johnston, Nucl. Instr. and Meth. 157 (1978) 461.
- [7] Iwao Ogawa, Tadayoshi Doke, Masahiro Tsukada, Nucl. Instr. and Meth. 13 (1961) 169.
- [8] H. Sann, H. Damjanschitsch, D. Hebbard, J. Junge, D. Pette, B. Povh, D. Schwalm, D.B. Tran Thoi, Nucl. Instr. and Meth. 124 (1975) 509.
- [9] H. Timmers, T.R. Ophel, R.G. Elliman, Nucl. Instr. and Meth. B 156 (1999) 236.